

The Effect of Environmental Conditions on Tropical Deep Convective Systems Observed from the TRMM Satellite

BING LIN, BRUCE A. WIELICKI, PATRICK MINNIS, LIN CHAMBERS, KUAN-MAN XU, AND YONGXIANG HU

Sciences Directorate, NASA Langley Research Center, Hampton, Virginia

ALICE FAN

SAIC, Hampton, Virginia

(Manuscript received 6 September 2005, in final form 14 March 2006)

ABSTRACT

This study uses measurements of radiation and cloud properties taken between January and August 1998 by three Tropical Rainfall Measuring Mission (TRMM) instruments, the Clouds and the Earth's Radiant Energy System (CERES) scanner, the TRMM Microwave Imager (TMI), and the Visible and Infrared Scanner (VIRS), to evaluate the variations of tropical deep convective systems (DCSs) with sea surface temperature and precipitation. The authors find that DCS precipitation efficiency increases with SST at a rate of $\sim 2\% \text{ K}^{-1}$. Despite increasing rainfall efficiency, the cloud areal coverage rises with SST at a rate of about $7\% \text{ K}^{-1}$ in the warm tropical seas. There, the boundary layer moisture supply for deep convection and the moisture transported to the upper troposphere for cirrus anvil cloud formation increase by $\sim 6.3\%$ and $\sim 4.0\% \text{ K}^{-1}$, respectively. The changes in cloud formation efficiency, along with the increased transport of moisture available for cloud formation, likely contribute to the large rate of increasing DCS areal coverage. Although no direct observations are available, the increase of cloud formation efficiency with rising SST is deduced indirectly from measurements of changes in the ratio of DCS ice water path and boundary layer water vapor amount with SST. Besides the cloud areal coverage, DCS cluster effective sizes also increase with precipitation. Furthermore, other cloud properties, such as cloud total water and ice water paths, increase with SST. These changes in DCS properties will produce a negative radiative feedback for the earth's climate system due to strong reflection of shortwave radiation by the DCS. These results significantly differ from some previously hypothesized dehydration scenarios for warmer climates, partially support the thermostat hypothesis but indicate a smaller magnitude of the negative feedback, and have great potential in testing current cloud-system-resolving models and convective parameterizations of general circulation models.

1. Introduction

Large cloud-climate feedback uncertainties limit the accuracy of current general circulation models (GCMs) for predicting the response of the earth's climate to increasing CO_2 concentration within the atmosphere. Current estimates of climate change for a doubled- CO_2 atmosphere, global mean temperatures increase between 1.5 to 4.5 K (Albritton et al. 2001), have remained virtually unchanged for two decades. Incomplete knowledge of cloud properties and their variations with environmental conditions is the major reason

for the large uncertainty. Some of the most important issues related to cloud feedbacks are recounted below. More detailed discussion of cloud feedbacks can be found in the critical review of Stephens (2005).

To date, most knowledge of cloud feedbacks is from observations of low clouds, specifically cloud liquid water path (LWP) or its directly associated parameter—optical depth (τ). Satellite observations equatorward of 60° latitude suggest that τ variations with temperature are strongly dependent on latitude and can be both negative and positive (Tselioudis et al. 1992). Ground-based measurements over midlatitude (Del Genio and Wolf 2000) and polar regions (Lin et al. 2003) support these satellite results and find that it is mainly the change of cloud thickness, not of adiabatic cloud water content, that causes the LWP variation. The base and

Corresponding author address: Dr. Bing Lin, MS 420, NASA Langley Research Center, Hampton, VA 23681-2199.
E-mail: bing.lin@nasa.gov

top heights of low clouds are significantly coupled with boundary layer moisture during warm seasons.

For high clouds, especially tropical deep convective systems (DCSs), there is almost no general agreement on their climate feedbacks. These DCSs basically have two parts: deep convective cores and cirrus anvil canopies. The cores are important for the atmospheric hydrological cycle because of their heavy precipitation and moisture transport to cirrus anvil clouds.¹ In contrast, DCS cirrus-anvil clouds, precipitating or not, are dominant in atmospheric radiation due to their large spatial coverage. Radiative properties, such as τ , LWP, ice water path (IWP), cloud temperature (T_c), effective cloud particle diameter (D_e), shortwave (SW) and longwave (LW) fluxes, and cloud areal coverage (A_c), of these convective systems are highly related to the underlying environments and large-scale dynamical states. Boundary-layer moisture convergence provides condensation potential, precipitation significantly removes hydrometeors, and detrainment from convective cores at the upper troposphere supplies moisture to form and maintain cirrus anvil canopies.

Based on satellite observations of tropical convective clouds, significantly different hypotheses of the responses of the convective systems to climate perturbations or sea surface temperature (SST) variations have been proposed (Ramanathan and Collins 1991; Lindzen et al. 2001). Large uncertainties in the properties of the cloud systems in the early satellite observations are one of the major reasons for deducing these contradictory hypotheses. Although the relationships among radiation, DCS, and SST have been investigated to some extent (e.g., Wallace 1992; Fu et al. 1992; Hartmann and Michelsen 1993, 2002; Lin et al. 2002), the dependence of DCS properties on broader atmospheric and oceanic environmental conditions, especially the parameters related to the hydrological cycle such as boundary layer moisture, precipitation, and rainfall efficiency are practically unknown due to lack of observations.

The variation of DCS with hydrological conditions is one of the keys in cloud feedback and climate studies.

¹ In the literature, especially in papers from the precipitation science community, precipitation systems are frequently separated into convective and stratiform precipitation areas. For tropical deep convective systems, the stratiform precipitation parts of the systems are usually close to convective towers and form thick anvil clouds (Houze 1993). Thus, the stratiform precipitation is also frequently called "anvil precipitation" in the literature as illustrated by Sud and Walker (1999). For thinner, more widespread clouds of DCS they, by definition, are cirrus clouds. For these reasons, this study uses "cirrus anvil canopies" to describe both thin and thick (precipitation or not) high clouds generated by and associated with deep convection.

Precipitation and precipitation efficiency have strong influences on the water budget of tropical convective systems. There have been many estimates of precipitation efficiency from observational data for thunderstorms and mesoscale convections (Braham 1952; Fankhauser 1988; Gamache and Houze 1983; Chong and Hauser 1989; Oury et al. 2000). Cloud modeling studies have also been used to evaluate the precipitation efficiency (Weisman and Klemp 1982; Lipps and Hemler 1986; Lucas et al. 2000; Shepherd et al. 2001; Tao et al. 2004). A review of these studies can be found in Ferrier et al. (1996). These studies usually just examined individual cases or cloud systems and had limited spatial and temporal coverage. For large-scale observations, Lau and Wu (2003) used new-generation satellite data of the Tropical Rainfall Measuring Mission (TRMM) to evaluate the residence time, a value inversely proportional to precipitation efficiency, of warm rain clouds over tropical oceans. Del Genio and Kovari (2002; hereafter DGK) made a study of the variation of tropical clouds with environmental conditions including precipitation efficiency using the new-generation satellite measurements. They analyzed effective size and albedo variations of tropical storms (precipitating clouds) using the Clouds and the Earth's Radiant Energy System (CERES) TRMM measurements and the TRMM Microwave Imager (TMI) precipitation product within 15° latitudes of the equator and found that, although precipitation efficiency may increase with SST as an efficiency index suggested, storms were generally bigger and brighter in warmer SST conditions. They further extended these TRMM results to modeling studies and evaluated the observed storm behavior for cloud-climate feedbacks (Del Genio et al. 2005). Because of the importance of cirrus anvil clouds, precipitating or not, for radiation budgets and upper-tropospheric moisture fields, the climate feedbacks of the DCS as a whole remain unresolved from the DGK analysis. Furthermore, because that analysis used only 5 days of TRMM data while the precession cycle of the TRMM orbit is 46 days, the DGK study may have only observed a narrow portion of the tropical storm diurnal cycle in active storm regions. Aerosol loadings also affect cloud formation and lifetime. Increasing aerosols would reduce cloud particle size, suppress precipitation, and lead to a weak atmospheric hydrological cycle (Ramanathan et al. 2001; Breon et al. 2002). Since this study is focused on the variations of tropical convective clouds with temperature, the aerosol influences on precipitation, rainfall efficiency, and climate are left for future studies.

This study focuses on observations of the relationship between environmental conditions, especially SST and

precipitation, and tropical DCSs using TRMM satellite measurements. Both convective cores and cirrus anvil canopies (including nonprecipitating cirrus–anvil clouds) are considered. The effects of SST, precipitation, rainfall efficiency, and moisture supply on the areal coverage of DCSs are discussed. The next section introduces the datasets and analysis methods used in this study. Section 3 shows observations of DCSs in different environmental conditions. These observations are discussed in section 4. Section 5 summarizes this study.

2. Data analysis

TRMM data taken over oceans between 30°N and 30°S during January through August 1998 are analyzed in this study. The time period is determined by CERES data availability. The CERES TRMM observations captured a transition from strong El Niño (during early 1998) to normal (or weak La Niña) tropical climate conditions, which includes large tropical dynamic and thermodynamic variations for the development of deep convection. The profound changes in the large-scale circulations and convective patterns during this period provide evidence for the fundamental physics of DCS clusters. This study mainly considers statistical features of deep convective clouds and their related environmental conditions. Because the precession cycle of the TRMM satellite is about 46 days, the statistical properties calculated from the CERES TRMM period cover multiple full diurnal cycles of DCS clusters in the tropical regions. Three instruments on board the TRMM satellite are used in this analysis. They are CERES for broadband SW and LW radiation at a spatial resolution of about 10 km, the Visible and Infrared Scanner (VIRS) for narrowband visible (VIS) and infrared (IR) measurements of about 2-km resolution over a 720-km swath, and TMI for precipitation and cloud liquid water path estimations. The spatial resolution of TMI measurements varies from about 4.6 km \times 7.2 km to 9.1 km \times 63.2 km over a total swath width of 780 km. For precipitation and LWP estimates used here, the resolutions are about 4.6 km \times 7.2 km and 9.1 km \times 16.0 km, respectively.

The basic dataset is the CERES single scanner footprint (SSF) product. Because the CERES product collocates CERES broadband measurements with CERES narrowband cloud retrievals from VIRS, SW and LW radiative fluxes in the CERES SSF dataset are estimated from the angular distribution models (ADMs) for specific cloud/clear types including DCS clusters, which yields instantaneous $\sim 13 \text{ W m}^{-2}$ SW and $\sim 4.3 \text{ W m}^{-2}$ LW errors, values at least a factor of 2 smaller than those from the Earth Radiation Budget Experiment

(ERBE: Loeb et al. 2003). SST values used in this analysis, as in Lin et al. (2002), are from the Reynolds SST analysis (Reynolds and Smith 1994) taken from the SSF product.

The CERES project, using a VIS–IR–Solar IR split-window technique (VISST: Minnis et al. 1995, 1997, 1999, 2002), processes VIRS measurements to detect cloudy and clear skies and to estimate effective cloud top temperature (T_c) and height, cloud thermodynamic phase (P_{wi}), τ , D_e , IWP, and LWP. VISST is a sophisticated iterative algorithm that matches measured multi-spectral radiances to radiative transfer model-computed spectral radiances for a range of cloud microphysical and macrophysical properties. The CERES cloud properties derived from 2-km resolution VIRS pixels are convolved into TMI 37-GHz fields of view (FOVs) to minimize spatial and temporal collocation errors. DCS rainfall rate (RR) values, along with precipitation ice and liquid water paths, of Goddard level-2 standard products of TMI (Kummerow et al. 2001) are registered to the collocated data. The retrievals of the RR and precipitation ice and liquid water paths are based on microwave signals of precipitating clouds at TMI frequencies covering from 19, 21 to 37, and 85 GHz. Brightness temperatures at 85 GHz have strong scattering signals for precipitating ice particles, while the values at lower frequencies are affected by both scattering of precipitating liquid and ice hydrometeors and absorption of liquid water drops (precipitating or not). TRMM Precipitation Radar (PR) makes direct measurements of tropical precipitation compared to TMI that indirectly measures tropical rainfall from the microwave scattering and absorption signals of precipitation systems. However, there are a couple of reasons that we do not use PR data in the following analysis. First, the differences between TMI- and PR-estimated rainfall rates are small due to the calibration of TMI precipitation retrievals against PR observations. Our comparison of TMI and PR precipitation data (not shown) reveals that the differences are within $\sim 10\%$ of the estimates for the 8 months of data in all SSTs, which results in a similar estimation of rainfall efficiency and causes no change in our conclusions. Second, the storm profiles estimated from PR data are for precipitation-sized hydrometeors such as graupel, snowflakes, hailstones, large ice crystals, large aggregates, and rainwater drops. Generally, the PR cannot detect nonprecipitation-sized ice and water particles very well and has no retrievals; that is, there is no estimation of water and ice amounts for nonprecipitating clouds in PR-detected rainfall areas. Thus, the LWP and IWP values cannot be evaluated from PR data even in precipitation regions. On the other hand, TMI data provide the infor-

mation in rainfall areas. For nonrain areas, the combination of TMI and VIRS data gives a decent estimate of LWP and IWP (see below). Third, the swath of PR measurements is only ~ 215 km, less than the sizes of a large portion of DCS clusters, and can cause problems in analysis of large tropical deep convective systems.

Over DCS nonprecipitating areas, multilayer cloud properties are estimated using the algorithm developed by Lin et al. (1998a,b) for the collocated passive microwave, visible, and infrared satellite data (Ho et al. 2003). For ice-over-water cloud systems, the upper-layer cirrus clouds are detected by VISST, while the cloud properties of lower-layer water clouds, such as LWP and water cloud temperature, are estimated from microwave observations. At 37 GHz, TMI brightness temperatures increase with cloud liquid water path and decrease with cloud water temperature, but those at 85 GHz increase with cloud water temperature. Thus, combining TMI measurements at 37- and 85-GHz channels, the algorithm retrieves cloud LWP and water temperature simultaneously. The algorithm carefully selects the microwave absorption coefficients for water vapor and cloud liquid water to account for their variation with temperature and pressure (Lin et al. 2001), thus making it suitable for analysis of supercooled water within or below anvils. Combining both VIRS total water path (LWP + IWP) and TMI LWP retrievals, IWP values are estimated for cirrus anvil clouds, especially under multilayer conditions (Ho et al. 2003; Lin and Rossow 1996). Besides these cloud properties, other TMI retrievals, such as column water vapor and near sea surface wind speed, are also merged with the CERES VIRS products (Ho et al. 2003).

After collocating the CERES cloud products from VIRS and TMI passive microwave measurements, we further match the data with the CERES SSF product for SW and LW fluxes. Since the FOVs of microwave 37-GHz measurements and CERES observations are similar in size, their footprints usually do not have closed convolutions. Weighted matches are used to merge CERES and TMI data. For each TMI pixel of DCS clusters, all CERES measurements within a 15-km radius of the center of the microwave pixel are considered as matched CERES pixels. The average SW and LW fluxes for the matched CERES pixels, weighted by their proximity to the TMI footprints, are calculated to represent the radiative properties of the DCS clusters that are covered by the TMI FOV.

The main ancillary data, such as wind vector (\mathbf{V}) and atmospheric temperature profile $T(z)$, are obtained from European Centre for Medium-Range Weather Forecasts (ECMWF) data assimilation products. Since the ECMWF analysis used here does not assimilate

TABLE 1. Data sources and geophysical properties obtained from each source.

| Sources | Properties |
|--------------------------|--|
| CERES SSF | A_c , albedo, SW and LW fluxes, SST under clear/cloudy, dry/moist conditions |
| CERES VIRS cloud product | A_c , T_c , P_{wi} , τ , D_e , IWP, LWP |
| TMI | Rain clouds: A_c , RR, precipitation LWP/IWP nonrain regions: A_c , LWP, WS, WV_L , E_s |
| ECMWF | \mathbf{V} , $T(z)$ |

TRMM measurements, ECMWF data are independent of our TRMM data. The wind divergences near sea surfaces are calculated from the ECMWF directional wind speed values with 6-h temporal and $0.5625^\circ \times 0.5625^\circ$ spatial resolutions. To obtain a smooth and reliable convergence field in representing preferential environmental conditions of moisture supply for DCS development, $1^\circ \times 1^\circ$ grid box means of the divergence values are used in this analysis. Large-scale moisture convergence is calculated based on the wind vector and the water vapor amount (WV_L) in the lowest 500 m of the atmosphere retrieved from TMI microwave measurements using the algorithm developed by Schulz et al. (1993). The accuracy of the satellite estimates of WV_L for each TMI pixel is about 0.6 kg m^{-2} , which is generally less than 10% of the water vapor amount and about 20% of the natural variability of the vapor amount over tropical oceans. With the boundary layer moisture amount [or top-of-atmosphere (TOA) microwave radiances], near-sea-surface air humidity can also be estimated from TMI measurements (Schulz et al. 1997). With the air humidity and near-sea-surface wind speed values estimated from TMI, sea surface evaporation rates (E_s) are calculated using a bulk formula (Fairall et al. 1996). Evaporation is a part of the total moisture supplied by the boundary layer to DCS clusters. Table 1 summarizes all data sources and the major properties provided.

To use TRMM data in detecting and analyzing tropical DCS, we first search for cold precipitating cloud clusters (CPCCs) within the combined TRMM data. A CPCC has at least one precipitation cell (minimum of two consecutive TMI precipitating pixels at 85 GHz to classify as a precipitating cell) with a thermal IR brightness temperature (T_{bIR}) colder than 245 K and a cloud-top height above 6 km. The clouds with cold tops ($T_{bIR} < 270$ K) or heights above 6 km around the precipitation cells are defined as part of the cloud cluster. Furthermore, any neighbor pixels of the cluster, precipitating or not, which satisfy the same cold top or height requirements, are also considered as part of the cluster.

In other words, a CPCC is a continuous cloud canopy with cold precipitating cells and possible cold nonprecipitating cirrus-anvil clouds. A DCS, in this study, is defined as a CPCC that has at least one rainfall cell with T_{bIR} colder than 218 K. The 218-K threshold is somewhat arbitrary. A nearby threshold such as 220 or 215 K would give results similar to those obtained here. These coldest rainfall cells represent deep convective cores, and other rain cells and nonprecipitating clouds within the DCS may be characterized as precipitation anvils and nonrain cirrus-anvil canopies, respectively. Detailed discussion about the DCS definition and detection techniques can be found in Machado et al. (1998). This study extends the technique through use of rainfall data from satellite microwave measurements. Since we will frequently discuss areas of DCS clusters, we introduce effective size (or radius) of DCS here. The effective size of clouds (such as DCS clusters and rainfall cells) is defined as the radius of a circle with an area equal to that of the clouds analyzed.

3. Results

Tropical deep convective clusters are very complicated systems. Their frequency and intensity are related to many environmental parameters. This section statistically evaluates the main DCS properties as a function of individual environmental parameters first, then considers the interconnections among these environmental conditions. Note that, since DCS clusters and their related environments are strongly nonlinear systems, our statistical approach cannot capture all of the variability of these systems. The statistical results here may represent the first-order (or the near-linear parts of) variations of DCS with environmental conditions.

Figure 1 shows the frequency distribution of DCS clusters as a function of SST. About 70 000 DCSs were detected in the 8 months of data. Some of these DCSs were observed by TRMM multiple times since the lifetime of these DCS clusters is generally much longer than that of the TRMM satellite orbital cycle. The large DCS database gives us large statistical samples of DCS clusters for most tropical SST conditions except for extremely cool and warm cases. As expected, a sharp peak frequency (about 35% of the total) of DCS clusters occurs around 302 K because large areas of the sea surface at that temperature have favorable conditions for DCS development. There are fewer regions with SST above 304 K, so the DCS number decreases. Tropical areas with SST below 298 K are generally distant from the intertropical convergence zones (ITCZs) and have much fewer DCSs (<15% of the total).

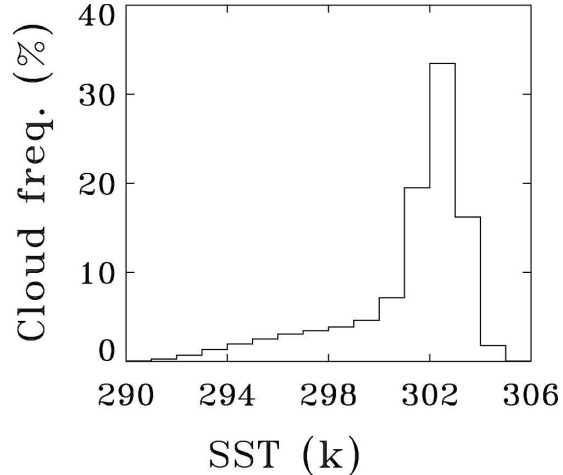


FIG. 1. DCS frequency distribution as a function of SST.

a. Sea surface temperature, rainfall rate, and DCS

As mentioned earlier, SST and precipitation play important roles in regulating DCS clusters. The variations of DCSs with their environmental conditions are very complicated. They are not only a function of SST and rainfall rate, but also functions of SST gradient, wind field, and moisture convergence, etc. We discuss SST and RR in this section and leave the other factors for later since precipitation, DCS, and SST may be more closely linked than other variable combinations.

Figure 2 shows how DCS cluster effective radius changes with the average SST under the DCS. The variation of effective DCS radius with SST for the temperature range from 290 to 305 K is not easy to understand. It may be largely related to the spatial distribution of DCS clusters. In the most-frequent DCS areas (300–304-K SST), there is a small positive trend of DCS size with SST. DGK found that the mean storm area increases significantly with SST in these SST regions. For lower SSTs (294–300 K), DCS size decreases with increasing SST. As mentioned above, the environmental conditions at these temperatures are actually much less favorable to produce deep convection. The largest averaged DCS clusters associated with SSTs around 294 K are not driven by thermodynamics (or SST), instead they are mainly caused by a few big tropical storms or midlatitude frontal systems mixing with a few small DCSs developed in these regions, as discussed by Hartmann and Michelsen (2002). Thus, if weighted by the frequency of tropical DCS clusters, the decrease of DCS size with SST would be removed as shown for DCS coverage (cf. Fig. 6 below). In contrast to the large DCS size in areas with SST around 294 K, the average DCS size is much smaller in deep tropical (high SST) areas, where both small developing and decaying

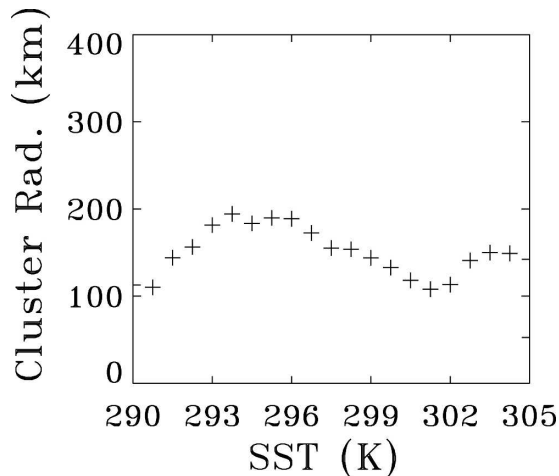


FIG. 2. DCS cluster effective size vs SST.

and large mature DCS clusters are frequently found. The evidence for this explanation can be seen in Figs. 1 and 2, that is, more and smaller DCS clusters in warm ($> \sim 300$ K) areas and fewer, but bigger, DCS in cooler ($< \sim 295$ K) regions.

The average rainfall rates of DCS clusters (Fig. 3) generally increase with SST, as expected. The relative change in RR with SST is about $4.4\% \text{ K}^{-1}$. When SST increases, the atmospheric temperature, especially that in the boundary layer, generally rises, enhancing the potential for more water vapor that would be available for convective systems. That is, the rainfall rates of these DCS clusters should grow with SST. The clear positive relationship between DCS effective radius and rainfall rate (Fig. 4) further demonstrates that DCS clusters with heavier precipitation are generally larger than those with lighter rainfall. Note that the sizes of

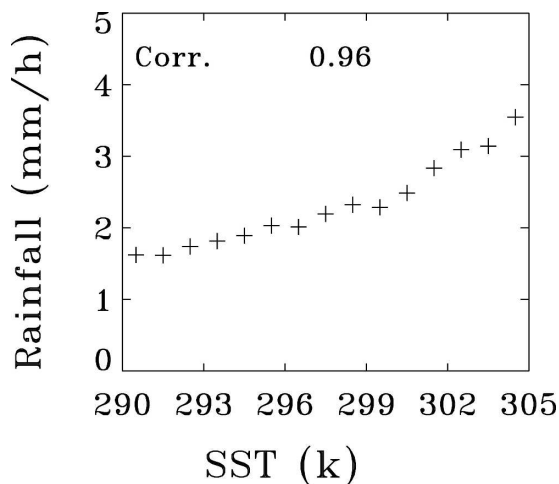


FIG. 3. Averaged DCS rainfall rates vs SST.

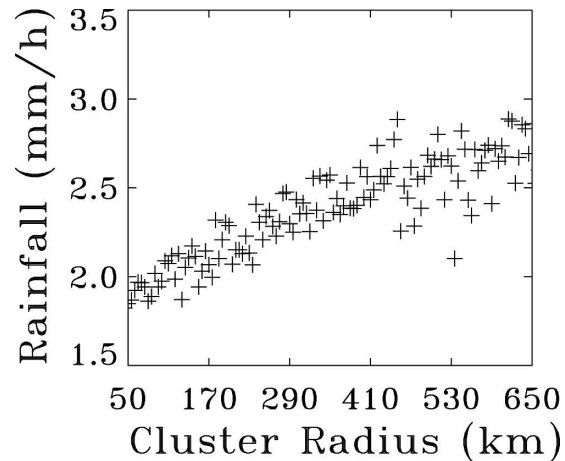


FIG. 4. The relationship between DCS effective size and rainfall rate.

the biggest DCS clusters (effective radius greater than about 450 km) may be underestimated owing to the limitation of the TMI swath. Thus, for the whole Tropics, rainfall rate increases with SST, and the heavier the precipitation of DCSs, the bigger the size of DCSs. Combining Figs. 2–4 and considering the complex variations of the DCS size with SST and our previous discussion about the cause of the decrease in the cluster size for SST between 294 and 300 K (Fig. 2), it is difficult to make any conclusions that greater rainfall rates caused by increasing SST would reduce the cluster size and detrainment of tropical DCS, as suggested by Lindzen et al. (2001).

The average ratio of the DCS rain area to the total DCS cluster area is small ($\sim 30\%$; Fig. 5). Combining the nonrain cirrus–anvil clouds of DCS clusters with the cirrus clouds not associated with the DCS clusters de-

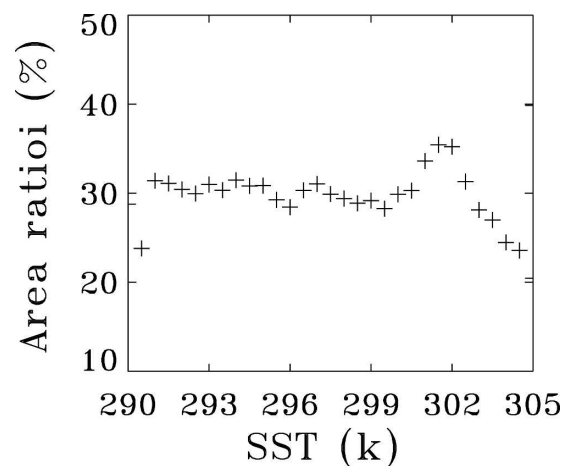


FIG. 5. The ratio of rain area to total area of DCS clusters.

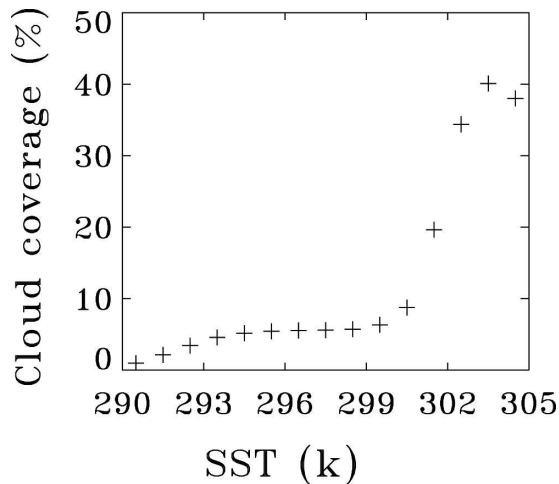


FIG. 6. The mean DCS areal coverage averaged in each 1-K SST interval.

tected here (not shown) clearly indicates that nonprecipitating tropical high clouds dominate the areal coverage of tropical high clouds and have the most influence on high-cloud radiation and climate feedback. The high values of the DCS rain-cluster area ratio at SST around 301 K may reflect the fact that relatively more developing DCSs grow in the warm sea areas. The anvil canopies of these premature DCS clusters may not be fully developed.

Figure 6 shows the mean DCS areal coverage averaged in each 1-K SST interval over all tropical oceans. Combined with Fig. 1, this result indicates that the areal coverage, not just the occurrence frequency, of DCSs is much higher in warm environments than in cool conditions. The average rate of increase in DCS areal coverage with SST is about $2.8\% \text{ K}^{-1}$. Although strongly

precipitating clouds can more effectively remove the atmospheric moisture transported into convective zones under warmer conditions, the areal coverage of DCS still increases with SST, suggesting more moisture from convective cores may be transported to the upper troposphere and cirrus anvil clouds in warmer environments. The variation of DCS areal coverage with SST is clearly nonlinear. For low SST ($<299 \text{ K}$) the DCS areal coverage increases by $\sim 0.46\% \text{ K}^{-1}$. At SSTs above 299 K, DCS areal coverage sharply increases at a rate $\sim 7\% \text{ K}^{-1}$. This rise is related to intensified convective activity and increased moisture transport from the boundary layer to the upper troposphere in these warm convergence zones. Further discussion of this issue will be given later.

b. Cloud total water path and ice water path

The SST dependencies of DCS total water path (WP) and IWP are shown in Fig. 7. For nonprecipitating clouds (Fig. 7a), both WP and IWP values increase with SST for warm (SST $> 299 \text{ K}$) conditions. Although the mean values of WP are relatively invariant at lower SSTs, the average IWP diminishes with decreasing SSTs, indicating that the DCSs over colder water may be less vigorous and pump less of the available water into the upper troposphere than their warm water counterparts. When both nonprecipitating and precipitating DCS clouds are considered, the WP and IWP values rise greatly from those of nonprecipitating clouds, except in the coolest regions (Fig. 7b). The large differences in the mean WP and IWP values between whole DCS clusters and their nonprecipitating portions reveal the importance of precipitation for the hydrological cycle: very infrequent occurrence and very large water and ice amount (cf. Lin and Rossow 1997). Like

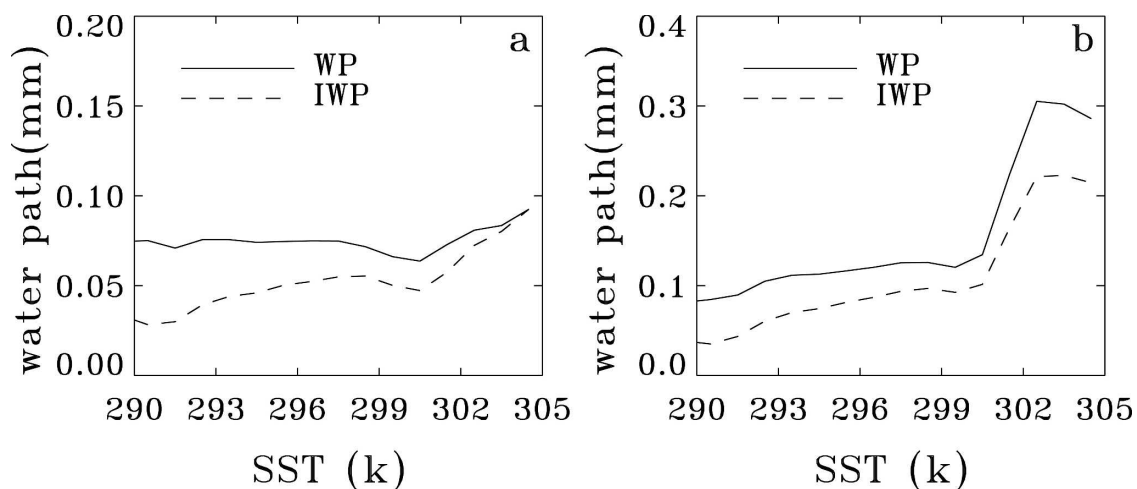


FIG. 7. DCS WP and IWP values for (a) nonprecipitating clouds and (b) whole DCS clusters.

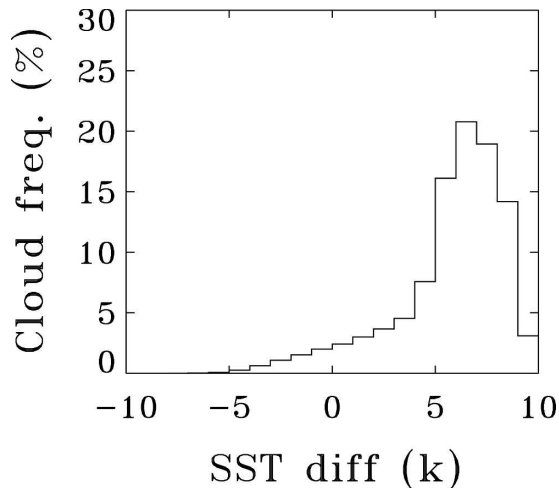


FIG. 8. As in Fig. 1 except for SST difference.

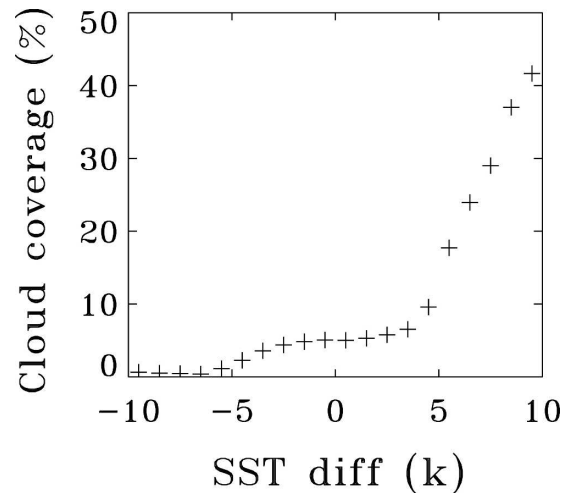


FIG. 9. As in Fig. 6 except for SST difference.

the IWP for the nonprecipitating DCS clouds, the mean IWPs for whole DCS also increase with SST. The increase in IWP is consistent with the mean cirrus-anvil top height changes of DCS clusters (not shown here). Thus, it can be seen that DCS clusters generally thicken with increasing SST.

c. Sea surface temperature difference and wind convergence

As discussed above, DCS development depends strongly on the local SST underneath the cloud clusters. Large-scale SST variability, such as its horizontal gradient between the DCS location and the remote cool subtropics, also play important roles in regulating DCS clusters. Variations in SST gradients may, at least partly, account for changes in the strength of general convective activity in the convergence zones and the Walker and Hadley cells. In short, the large-scale meridional circulation strengthens as the temperature differences increase between the warm DCS areas and the cool subtropics. The temperature differences between the SST values under DCS clusters and the mean SST values over the northern and southern zones between 25° and 30° latitude are used here to quantify the effects of the large-scale SST gradient on DCS. Figure 8 shows the frequency distribution of DCS clusters with the SST difference. Most DCS clusters (~75%) developed in large SST difference (>4 K) conditions. A few DCS clusters are found with negative SST differences. They are located over cool subtropical regions and most of them arrived there as a result of advection from mid-latitude or equatorial areas (Hartmann and Michelsen 2002). A strong positive relationship, with a correlation coefficient of 0.89, exists between the DCS areal cov-

erage and the SST difference, especially for high temperature difference cases (Fig. 9). For areas with SST differences between 4 and 10 K, the DCS cloud coverage sharply increases from about 7% to 40%.

DCS clusters have a broad frequency distribution with the divergence of the large-scale low-level wind fields (Fig. 10). The magnitudes of the estimated divergences are small owing to the nature of vertical motion in the spatial and temporal scales of this analysis. Negative divergence (or convergence) conditions generate more DCSs than positive conditions. Since most areas of tropical oceans are under divergence conditions, the small shift in the DCS probability distribution to the convergence regime indicates the significant importance of large-scale forcing on the development of DCS. Convergence conditions favorably support the

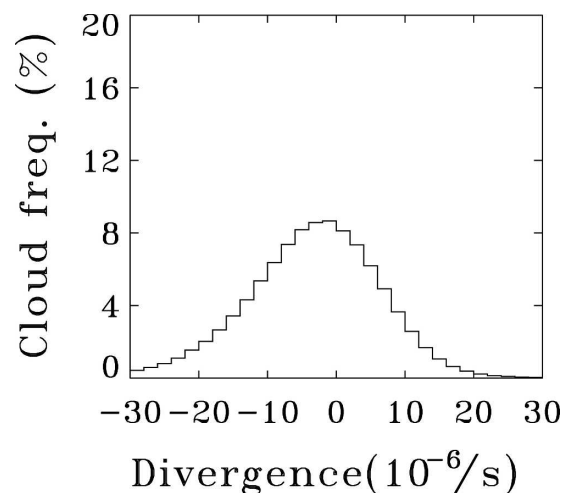


FIG. 10. As in Fig. 1 except for divergence.

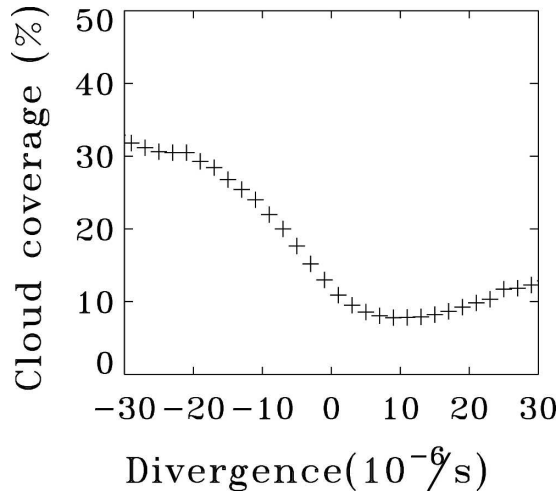


FIG. 11. As in Fig. 6 except for divergence.

moisture needed for triggering, developing, growing, and maintaining convective systems. Condensation of water vapor into water and ice hydrometeors of convective systems in the upper troposphere releases latent heat, which is the main energy source required for DCS development. The importance of convergence to tropical deep convection can also be seen from the mean DCS area coverage plotted as a function of divergence (Fig. 11). In large-scale convergence regimes, DCS cluster areal coverage generally increases with the convergence and changes from $\sim 10\%$ to $\sim 30\%$ for convergence values varying from 0 to about $30 \times 10^{-6} \text{ s}^{-1}$, while for divergence regimes, DCS cloud cover is much smaller with an average value of $\sim 8\%$.

d. Intercorrelations of environmental parameters

Previous sections discussed complicated relationships among DCS effective size and areal coverage and environmental variables such as SST, SST difference, divergence, and rainfall. These environmental variables could provide favorable large-scale conditions for DCS development, growth, and maintenance, and also interact with DCS clusters. Gregarious characteristics are common phenomena for tropical convection (Mapes 1993). For example, divergence and rainfall conditions not only directly affect but also are the results of tropical deep convection. Furthermore, these environmental variables are not fully independent. To the first order, most of these variables are related to SST.

Figure 12 shows the nearly linear relationship between the averaged SST and SST difference for the 8-month tropical data. Over a large part of the SST range, there are positive SST differences between the areas of DCS cluster developments and the cooler sub-

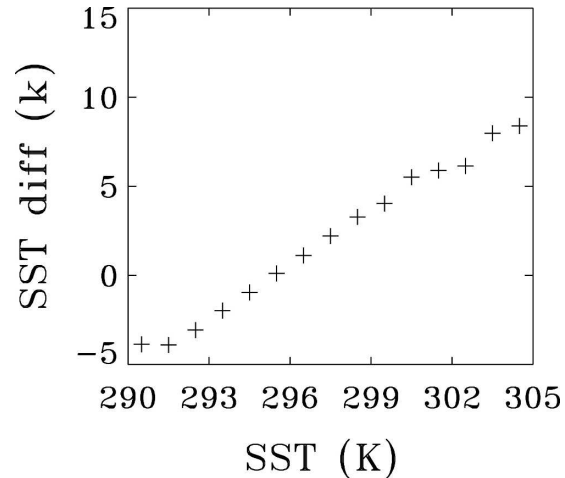


FIG. 12. Variations of SST difference on SST.

tropical regions. Statistically, most DCS clusters develop in conditions with big ($>3 \text{ K}$) SST differences or in environments with high SSTs (cf. Fig. 1). For areas having the most frequent DCS occurrences (SST $\sim 302 \text{ K}$), deviating from the linear relationship of SST and SST difference is evidence although they are correlated. Generally, the SST difference and SST for current climate are entwined. The combination of positive SST difference and high SST maintains tropical general circulations and provides favorable large-scale dynamic and thermodynamic environments for development of deep convection. As mentioned before, in low SST areas (also negative SST difference), there are few locally generated DCS clusters; a large portion of them develop elsewhere and advect into the low SST region.

Convergent winds force the vertical transport of boundary layer moisture into clouds in the areas with the most frequent occurrence of DCS clusters (Fig. 13). Although large oceanic areas maintain dynamical conditions that horizontally remove boundary-layer water vapor (i.e., divergence conditions), the relatively smaller tropical convergence areas develop more DCS clusters than the larger divergence areas (cf. Figs. 10, 11, and 13). In the warmest (SST $> \sim 304 \text{ K}$) regions, the convergence is slightly weaker and the DCS areal coverage is slightly lower (Fig. 6) than their counterparts in slightly cooler (SST $\sim 302 \text{ K}$) regions. The exact reason for this DCS inflection point is not clear. Tompkins (2001) suggests that the DCS feature could result from a self-aggregation of the clouds caused by a feedback between convection and the water vapor field. Detailed studies of the dynamics and thermodynamics of these warmest sea regions are needed. In divergence zones, there are fewer large DCS clusters. The presence of strong DCS clusters in those instances may change

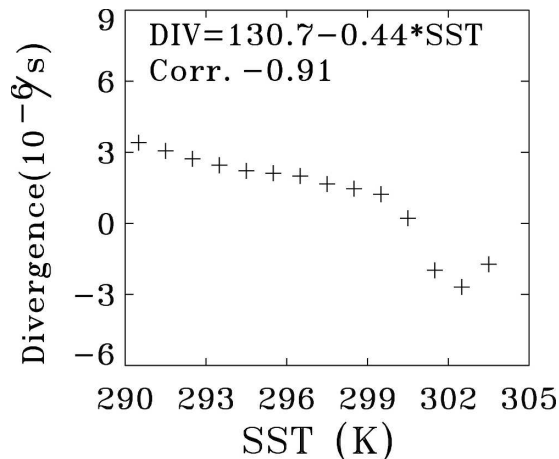


FIG. 13. Divergence vs SST.

the local normal climatological wind fields and produce local low pressure environments that bring moisture for continued DCS development. Figure 13 also shows that the climatological divergence and SST values are correlated. The higher the SST, the smaller the divergence (or the larger the convergence). Since increasing CO₂ concentration in the atmosphere likely produces warmer SSTs, and the purpose of this study is to evaluate cloud–climate feedbacks, we mainly focus on DCS variations with SST changes in the following discussions. The change in the entwined relationships among SST, SST gradient, and divergence in the changing climate and their effects on DCS are assumed to be some of the responses to rising SSTs. Actually, the influences of the change in large-scale dynamics on DCS are beyond the scope of the current study and will be analyzed in the future.

4. Discussion

a. Moisture balance

As in many previous studies, we find a significant increase of tropical deep convective clouds with SST. The cloud WP and IWP also increase with SST (cf. Fig. 7). Compared with the DCS size over cooler waters, the average DCS cluster size is smaller over warm (SST > 299 K) regions, but the total number of DCSs is so much greater that the fractional areal coverage of DCS clusters over these warm regions is still significantly higher (Figs. 1, 2, and 6) than over colder tropical regions. With increasing SST, mean rainfall rates increase, and the increased rainfall is positively correlated with DCS cluster size. The increase of DCS areal coverage with SST and large cluster sizes for strong rainfall are not consistent with the scenario of Lindzen

et al. (2001), which hypothesizes that deeper convection under warmer sea conditions could cause higher rainfall efficiency that would result in the reduction of DCS area coverage in warmer environments. So far, the results presented in this study do not support such an effect.

To evaluate the relationships of SST, rainfall efficiency, and DCS area coverage, we estimate rainfall efficiency here. There is no standard quantitative definition of rainfall efficiency (cf. DGK; Tao et al. 2004). This study defines the efficiency as the ratio of RR to the boundary layer moisture supply (M_s) of tropical convective systems. That is, the ratio of the water removed by the convection to the water transported into the DCS cluster from the planetary boundary layer (PBL). Here M_s can be expressed as

$$M_s = -\partial Q_b / \partial t + E_s - \nabla \cdot Q_b \mathbf{V}, \quad (1)$$

$$= -\partial Q_b / \partial t + E_s - \nabla Q_b \cdot \mathbf{V} - Q_b \nabla \cdot \mathbf{V}, \quad (1a)$$

where Q_b , E_s , and \mathbf{V} are water vapor amount, sea surface evaporation, and horizontal wind vector within the PBL, respectively. The first term on the right-hand side of (1) is the water vapor supply to DCS clusters due to the change in moisture within the boundary layer, the moisture tendency. The third term is the horizontal water vapor transport and can be separated into water vapor gradient and convergence contributions as shown in (1a).

The local evaporation is important in maintaining the PBL moisture amount and generally depends on relative humidity, temperature, and wind speed. The transport of the evaporated moisture from large sea surface areas, even from remote places, to active DCS regions provides a major part of the moisture supplies for convective development. Although WV_L is estimated from TRMM data for the lowest 500 m of the atmosphere, the exact thickness of the PBL for supplying moisture to DCS clusters is very difficult to obtain. It depends on many factors and may vary from one system to another. Thus, the 500-m thickness is used here, following DGK.

Figure 14 shows WV_L versus SST, along with the results of theoretical calculations based on a constant (78%) relative humidity and an atmospheric lapse rate of 6.5 K km⁻¹. The theoretical results are very close to the observed values, especially for higher SST cases. The boundary layer moisture changes from about 4 mm at 291 K to around 11 mm at 304 K, values that are about 1–2 orders of magnitude higher than IWP (Fig. 7), even for IWP values including precipitation-sized hydrometeors. Thus, the reservoir of boundary layer moisture for upper-tropospheric cloud formation in large spatial and long temporal scales is huge, and DCS

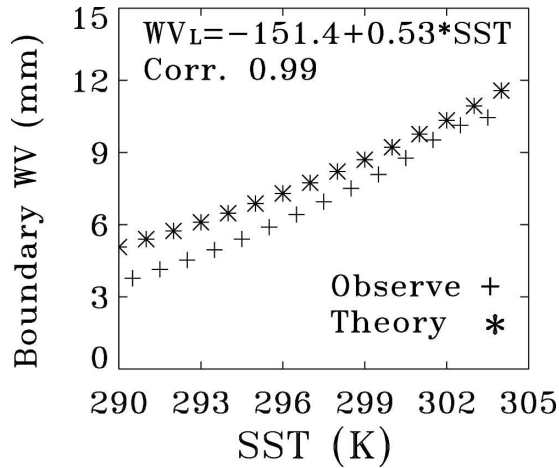


FIG. 14. Lowest 500-m atmospheric water vapor amounts observed by TRMM (+) and calculated through a constant relative humidity (*).

areal coverage may not be directly affected by tropical precipitation. Of course, for individual precipitating cells, the atmospheric water path is extremely large, so the difference between the boundary layer moisture amount and the precipitation LWP and IWP (Lin and Rossow 1997) should not be so dramatic. To maintain the rainfall in DCS clusters, high WV_L values in precipitating areas must be supported by continuous moisture inputs from the large-scale environment to the local PBL.

The moisture tendency term is calculated from changes in local WV_L values estimated from the TRMM satellite. This tendency term is generally smaller than the moisture convergence term over convergence zones but very important for the DCS moisture supply over large-scale divergence areas. Finally, the moisture divergence can be estimated by a combination of WV_L values and near-sea-surface wind divergence fields from the ECMWF data. Over divergence areas ($SST < 299$ K), the moisture convergence (Fig. 15) is generally negative with small variations around $-10 \times 10^{-6} \text{ mm s}^{-1}$ with SST. Steady decreases in the wind field divergence and smooth increases of boundary layer moisture with SST may result in the small change in the moisture convergence. In active convection areas ($SST > 299$ K), the moisture convergence increases quickly from the negative value to a number as high as $\sim 30 \times 10^{-6} \text{ mm s}^{-1}$.

With the above discussion of boundary layer moisture, the rainfall efficiency (η : the ratio of rainfall rate to vertical moisture supply from the boundary layer) can be estimated as

$$\eta = RR/M_s = RR/(-\partial WV_L/\partial t + E_s - \nabla \cdot WV_L \mathbf{V}_L). \quad (2)$$

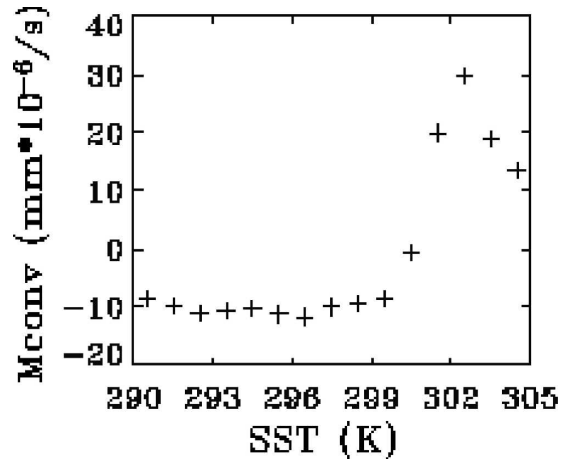


FIG. 15. The boundary-layer moisture convergence.

Since the layer of horizontal moisture transport to DCS clusters may be thicker than 500 m and the wind aloft is stronger than that of the lowest atmospheric layer, this study may underestimate the moisture supply of DCS clusters. On the other hand, since the PBL moisture budget is calculated in gridded boxes and cannot be estimated for each TRMM pixel due to the limitation of the ECMWF data and since the rainfall is evaluated for large DCS clusters in this study, the precipitation from small convective clouds in DCS gridded boxes may be missed. That is, this study may underestimate the removed water in our moisture budget analysis. Thus, the current estimate of rainfall efficiency may be close to the true η value for DCSs.

The rainfall efficiency as a function of SST obtained from the 8 months of TRMM data is plotted in Fig. 16. The averaged η values are pretty low ($\sim 35\%$), even for convergent areas (only from $\sim 20\%$ to 50%), and basically increase with SST. Most moisture supplied to DCS clouds is either converted to cloud liquid or ice water or injected into the upper troposphere, moisturizing that part of the atmosphere, and is not removed by precipitation processes of deep convection. For cool areas, rainfall efficiency variations are small and are generally around 20%. As expected, the rainfall efficiency increases sharply with SST under warm conditions. The rate of increase of η with SST is about $\sim 2\% \text{ K}^{-1}$ (or, relatively, $\sim 6\%$ of the averaged η per kelvin SST increase).

Although the rainfall efficiency increases with SST, there is no evidence of insufficient upper-tropospheric moisture for DCS cirrus anvil cloud formation. Actually, as shown before, the DCS area coverage increases with SST (Fig. 6), which means that the accelerated dehydration processes of DCS precipitation with increased SST are still not strong enough to reduce the

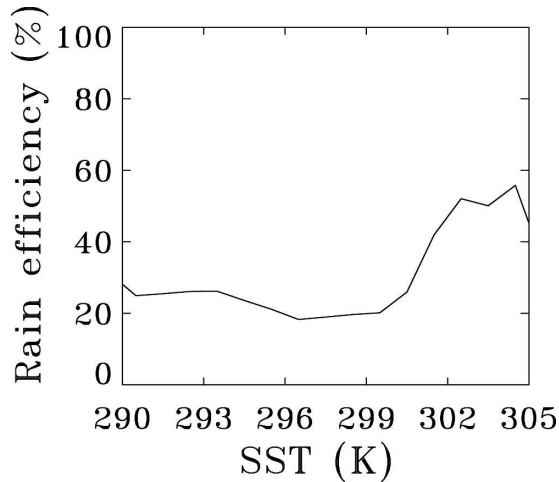


FIG. 16. DCS rainfall efficiency.

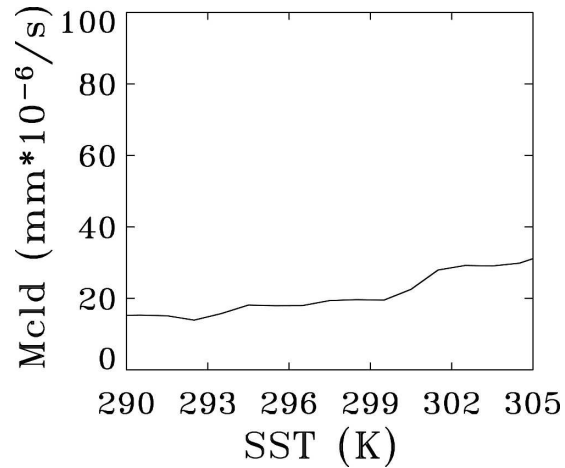
moisture transport to the upper troposphere and to lower the humidity in the region. The results show only the slightest hint of a decrease at 305 K, where sampling is minimal. A simple estimate finds that DCS clusters, on average, still obtain more moisture over warmer waters than under cooler conditions. The effective moisture transported to the upper troposphere for DCS cirrus anvil formation (M_{cld}), not precipitation, is the difference between the total boundary layer moisture supply and the moisture removed by rainfall; that is,

$$M_{\text{cld}} = M_s - \text{RR} = M_s(1 - \eta). \quad (3)$$

Thus, for a 1-K SST change, the change in cloud moisture transport ΔM_{cld} can be expressed as

$$\begin{aligned} \Delta M_{\text{cld}} &= \Delta[M_s(1 - \eta)] \\ &= \Delta M_s(1 - \eta) - M_s \Delta \eta \\ &= M_s[\Delta M_s/M_s(1 - \eta) - \Delta \eta]. \end{aligned} \quad (4)$$

The terms for DCS moisture supply, that is, the moisture tendency, evaporation, and moisture convergence terms, are all functions of temperature, humidity, and wind speed. The change in these terms with environmental temperature is basically related to the change of boundary layer humidity if wind fields are assumed to be invariant with SST. Thus, we use the change of boundary layer moisture to evaluate M_s variations with temperature. Under mean tropical conditions (SST ~ 298 K), a 1-K increase in surface temperature would cause a 6.3% relative change in boundary-layer water vapor amount when relative humidity is assumed to be a constant. Thus, the relative change in the moisture supply ($\Delta M_s/M_s$) in (4) would be about 6.3% K^{-1} without changes in wind fields. For the low rainfall efficiency observed ($\sim 35\%$) and the increasing rate of

FIG. 17. Moisture transport for DCS cirrus anvil clouds (i.e., $M_s - \text{RR}$).

rainfall efficiency with temperature (2% K^{-1}), ΔM_{cld} is clearly still larger than 0; that is, cloud moisture supply increases with temperature. For a 1-K temperature increase, the relative change of moisture transport for DCS clouds is

$$\begin{aligned} \Delta M_{\text{cld}}/M_{\text{cld}} &= \Delta M_{\text{cld}}/[M_s(1 - \eta)] \\ &= [\Delta M_s/M_s(1 - \eta) - \Delta \eta]/(1 - \eta) \\ &= \Delta M_s/M_s - \Delta \eta/(1 - \eta) \\ &\approx 6.3\% - 2\%/(1 - 0.35) \\ &\approx 3.0\%. \end{aligned} \quad (5)$$

This estimate means that for each degree of SST increase, the relative total moisture transport into DCSs increases about 6.3%. Within the 6.3% increased moisture transport, about half of the increased moisture is removed by increased rainfall efficiency and not actually used for cirrus anvil cloud formation. Although the estimated relative change ($\sim 3.0\% \text{K}^{-1}$) in the upper-tropospheric moisture (M_{cld}) fed to DCS cirrus anvil clouds with temperature is lower than that (6.3% K^{-1}) of total moisture supply for DCS clusters because of the increased rainfall efficiency at higher temperatures, the absolute amount of the moisture supply for cirrus anvil cloud development still increases. From TRMM, the observed change of $\sim 4.0\% \text{K}^{-1}$ (Fig. 17) in the moisture transport for DCS cirrus anvil formation (M_{cld}) not only has the same sign as our theoretical simple estimation, but also is quantitatively close to the estimated value (3% K^{-1}). So, generally, the higher the temperature in tropical environments, the wetter the tropical atmosphere, including the upper troposphere. This is consistent with the observed DCS area coverage increase in warm environments (Fig. 6).

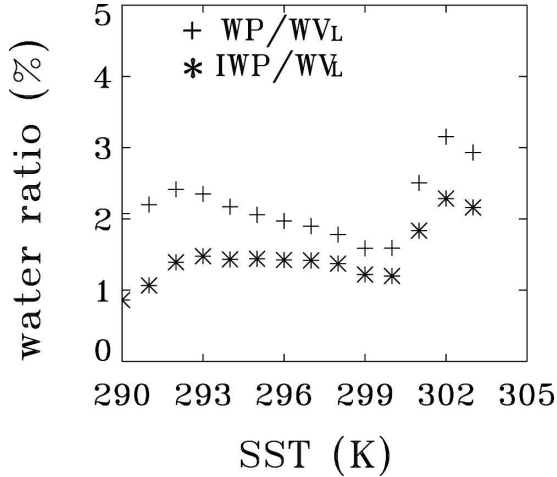


FIG. 18. Water ratio of cloud IWP (and WP) and boundary-layer water vapor amount.

If the relative change of DCS areal coverage were the same as that ($\sim 4.0\% \text{ K}^{-1}$) of the observed moisture transport (M_{cid}) for cirrus anvil clouds of DCS clusters, in other words, if there were no changes in the cloud formation efficiency with temperature, with about 25% of the average DCS areal coverage over the warm sea areas, the absolute rate of increase in DCS areal coverage would be about $1\% \text{ K}^{-1}$, which is much smaller than the observed rate ($\sim 7\% \text{ K}^{-1}$) in warm conditions. This estimated value of $1\% \text{ K}^{-1}$ is still within the range ($0.5\% \text{ K}^{-1} \sim 7\% \text{ K}^{-1}$) of the DCS change rate over cool and warm sea surface areas (cf. Fig. 6 and its discussion). With deepening of DCS clusters, the cloud formation efficiency, defined as the ratio of condensation rate to moisture transport for DCS cirrus anvil cloud formation, may change with temperature too. Although no quantitative estimates of the cloud formation efficiency are available in this study because it is impossible to obtain the upper-troposphere moisture sink rate (i.e., condensation rate) for DCS clusters, especially in the cirrus anvil regions, an indication of the cloud formation efficiency is studied here using the ratio of cloud IWP (or WP) to boundary layer moisture amount following DGK. With temperature increases in the high SST environments, the ratio of IWP to WV_L is almost doubled (Fig. 18). In cool environments (SST < 299 K), variations of the water ratio are minimal. The current water ratio values are much smaller than those of DGK, due mainly to the fact that our analysis includes both precipitating and nonprecipitating clouds while DGK only studied storm (i.e., precipitating) cases. The IWP values for precipitation pixels are generally at least an order of magnitude higher than those of nonprecipitating clouds. Despite the differences be-

tween the current and DGK analyses, the basic trends of the two observed water ratios are similar, suggesting significant increases of cloud formation efficiency with temperature. Thus, the large increase in DCS area coverage over warm water is no surprise.

b. Radiative effects of DCS clusters

The variations of DCS areal coverage with environmental conditions affect both water (humidification of upper troposphere) and energy (radiation) cycles. The DCS radiative feedback is usually defined as the change of radiation fields from clear sky to DCS conditions. Thus, the LW, SW, and net radiative forcings, F , for the atmosphere are

$$F_{\text{LW}} = (-\text{LW}_{\text{DCS}}) - (-\text{LW}_{\text{clr}}) = \text{LW}_{\text{clr}} - \text{LW}_{\text{DCS}} \quad (6a)$$

$$F_{\text{SW}} = (S - \text{SW}_{\text{DCS}}) - (S - \text{SW}_{\text{clr}}) = \text{SW}_{\text{clr}} - \text{SW}_{\text{DCS}} \quad (6b)$$

$$F_{\text{net}} = F_{\text{SW}} + F_{\text{LW}}, \quad (6c)$$

where S is the TOA solar radiation; SW_{clr} and SW_{DCS} values are CERES-measured TOA reflected solar radiation in clear and DCS conditions, respectively. Similarly, LW_{clr} and LW_{DCS} represent TOA outgoing longwave radiation under corresponding conditions. Generally, F_{SW} is negative and F_{LW} is positive since DCS clusters are brighter and colder compared to clear skies.

Actual development of DCS clusters may not be from a clear sky background. These cloud systems can grow from low cloud, moist, or partially cloudy conditions, as discussed by Lin et al. (2002). The DCS radiative feedback under these environmental conditions significantly differs from that under clear skies. To thoroughly analyze the radiative effects of DCS clusters, we introduce a generalized radiative forcing of clouds, G , which defines radiative forcing as the difference between DCS and existing environmental conditions. Thus, Eq. (6) becomes

$$G_{\text{LW}} = (-\text{LW}_{\text{DCS}}) - (-\text{LW}_{\text{env}}) = \text{LW}_{\text{env}} - \text{LW}_{\text{DCS}} \quad (7a)$$

$$G_{\text{SW}} = (S - \text{SW}_{\text{DCS}}) - (S - \text{SW}_{\text{env}}) = \text{SW}_{\text{env}} - \text{SW}_{\text{DCS}} \quad (7b)$$

$$G_{\text{net}} = G_{\text{SW}} + G_{\text{LW}}, \quad (7c)$$

where the “env” means the existing environmental conditions. We call these (G_{SW} , G_{LW} , and G_{net}) forcings the generalized forcings due to DCS development from an existing environmental condition.

Figure 19 shows DCS radiative forcings from envi-

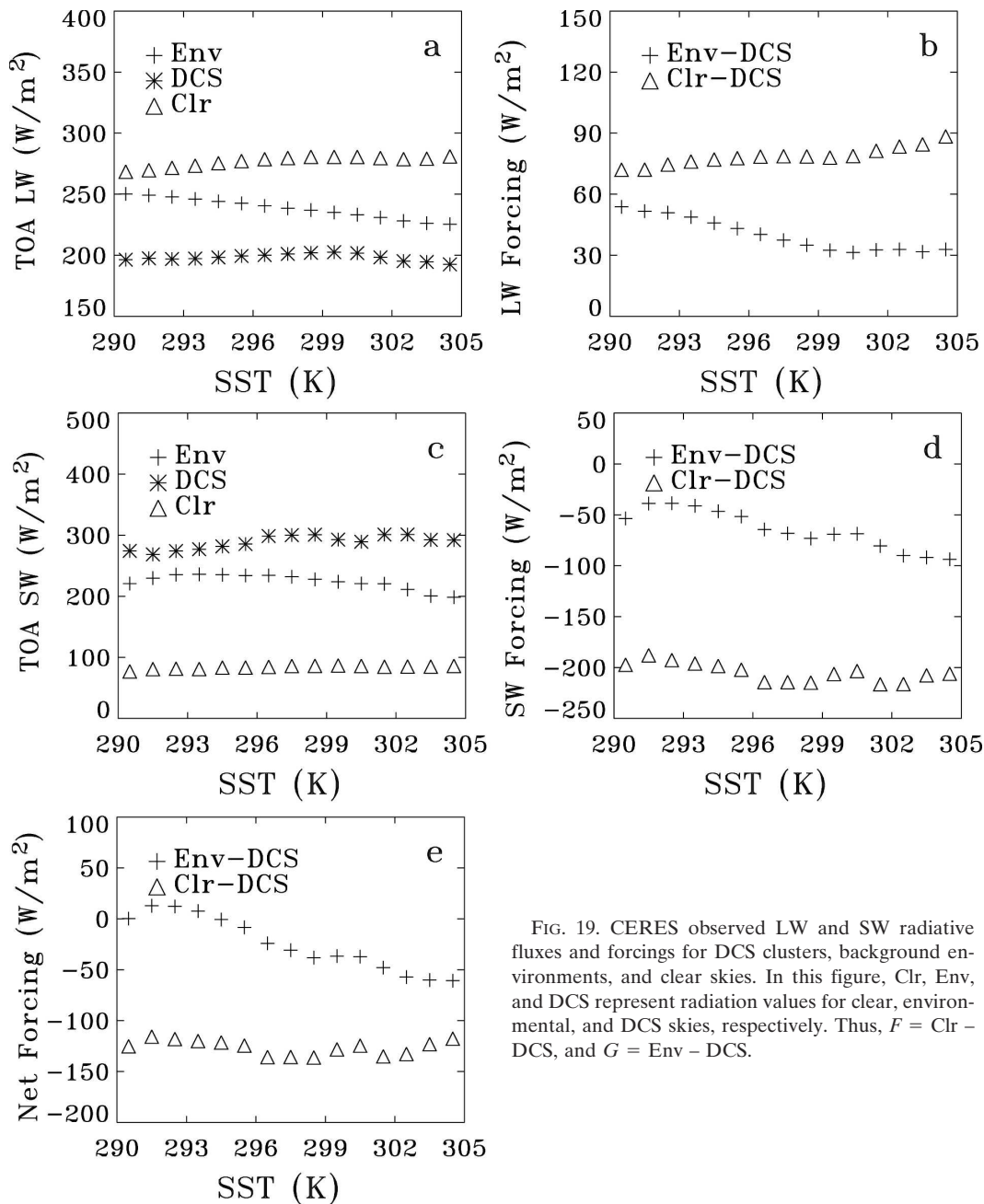


FIG. 19. CERES observed LW and SW radiative fluxes and forcings for DCS clusters, background environments, and clear skies. In this figure, Clr, Env, and DCS represent radiation values for clear, environmental, and DCS skies, respectively. Thus, $F = \text{Clr} - \text{DCS}$, and $G = \text{Env} - \text{DCS}$.

ronmental conditions, along with those from clear skies. The environmental condition is obtained from areas surrounding DCS clusters with the technique used by Lin et al. (2002) and Chambers et al. (2002). These environments are a mix of both clear and cloudy skies but include no high clouds. On average, these environments and high clouds occupy half of tropical oceans. From the figure, it can be seen that the reflected SW radiation for DCS clusters, environmental conditions, and clear skies is pretty uniform throughout the tropical

oceans (Fig. 19c). The outgoing DCS LW radiation also has minimal variability, indicating that the mean DCS top temperature is nearly constant (Fig. 19a). The decrease of LW_{env} from $250 W m^{-2}$ around 290-K SST to $225 W m^{-2}$ at high SSTs may be caused by a gradual increase in atmospheric moisture due to higher temperatures, while the rise in clear-sky LW with SST is clearly related to the atmospheric temperature. As expected, G_{LW} and G_{SW} are much smaller than F_{LW} and F_{SW} (Figs. 19b,d). The average net DCS radiative forc-

ing from environmental conditions is relatively weak (about -20 W m^{-2}) while the radiative forcing from clear conditions is strong and reaches about -125 W m^{-2} (Fig. 19e). If thin cirrus clouds not associated with DCS clusters are considered, the generalized net radiative forcing of high clouds will be even smaller. The G_{net} changes with temperature are about $-7 \text{ W m}^{-2} \text{ K}^{-1}$ and $-5 \text{ W m}^{-2} \text{ K}^{-1}$ for high SSTs and over the entire SST range, respectively. With DCS areal coverage about 25% over warm regions and the $-7 \text{ W m}^{-2} \text{ K}^{-1}$ change of net radiative forcing with temperature, the DCS-induced net radiative feedback is about $-1.75 \text{ W m}^{-2} \text{ K}^{-1}$ for the SST environments, which is smaller than that ($-4 \sim -6 \text{ W m}^{-2} \text{ K}^{-1}$) obtained by Ramanathan and Collins (1991) in the equatorial Pacific. Over all tropical oceans, the mean DCS net radiative feedback caused by temperature changes is about $-1.25 \text{ W m}^{-2} \text{ K}^{-1}$.

Generally, an increase of DCS areal coverage with SST would cause a negative radiative feedback. Since the average increase of DCS area coverage is about 2.8 \% K^{-1} and the mean DCS G_{net} is about -20 W m^{-2} (Figs. 6 and 19), the radiative feedback due to change in DCS areal coverage is about $-0.56 \text{ W m}^{-2} \text{ K}^{-1}$. Over warm regions, because the increase of DCS areal coverage is $\sim 7\% \text{ K}^{-1}$ and the DCS G_{net} is about -40 W m^{-2} (Figs. 6 and 19), the radiative feedback is about $-2.8 \text{ W m}^{-2} \text{ K}^{-1}$. Thus, the estimated feedback due to DCS area coverage in the warm regions is smaller than that of Ramanathan and Collins (1991). In terms of the tropical climate as a whole, it can be seen that the DCS radiative feedback over tropical oceans is much smaller than that obtained over the high-SST areas. Since this study only deals with DCS clusters, the generalized net radiative forcing due to changes in all tropical high clouds may be even smaller if thin cirrus clouds not associated with DCS clusters were included. The excluded thin cirrus clouds occupy about 5%–10% of the Tropics and are significant for cloud radiative forcing, although much less important than DCS clusters. Furthermore, our derived changes of DCS areal coverage with SST are only for the current climate; some of the apparent SST dependence of the DCS coverage may be related to a change in vertical velocity of the atmosphere as suggested by Del Genio et al. (2005), which does not automatically carry over to altered climates. Thus, the absolute values of our estimated negative feedbacks are likely to be the upper limits for actual climate changes.

5. Summary

This study uses the measurements taken during January through August 1998 from multiple TRMM sen-

sors, namely CERES, TMI, and VIRS, to evaluate the effect of environmental conditions on tropical deep convective systems. The focus is on the variation of DCS areal coverage with SST and precipitation. As expected, we find that not only rainfall rate but also rainfall efficiency increases with SST. The change of the efficiency is about $2\% \text{ K}^{-1}$, indicating that DCSs more effectively remove the moisture transported into the upper troposphere when the temperature gets warmer. Even with the increased rainfall efficiency, the DCS areal coverage increases with SST, especially when SST exceeds 299 K. In warm environments, both the boundary-layer moisture supply for deep convection and the moisture transported to the upper troposphere for cirrus anvil cloud formation increase with a rate $\sim 6.3\% \text{ K}^{-1}$ and $\sim 4.0\% \text{ K}^{-1}$, respectively. The rate of increase of the DCS areal coverage obtained from TRMM is about $7\% \text{ K}^{-1}$ in high-SST conditions. Besides the increased moisture transport for cloud formation, the changes in cloud formation efficiency are likely another reason for the large rate of increasing DCS areal coverage with SST. Although rainfall efficiency increases with SST, the dehydration process can only remove part of the increased moisture transport to the upper atmosphere and is not strong enough to overcome the increased moisture transport in warm environments. The increased moisture transport via enhanced convection moistens the upper troposphere and increases the DCS areal coverage. In addition to the DCS coverage, DCS cluster effective sizes also increase with increasing precipitation. Furthermore, other cloud properties, such as cloud total water and ice water paths, change positively with SST. These results significantly differ from the hypothesized dehydration scenario of Lindzen et al. (2001) for a warmer climate. Since the net radiative forcing due to DCS development from existing environmental conditions is about -20 W m^{-2} , the change of DCS with SST will produce a negative radiative feedback for the earth's climate system. This study partially supports the thermostat hypothesis but indicates a smaller magnitude of the negative feedback. Our observed results for DCS have great potential in testing current cloud- system-resolving models and GCM convection parameterizations. Future studies will concentrate on thin cirrus variations with temperature and the cloud formation efficiency to thoroughly understand moisture transformation from vapor to condensed forms and the change of DCS-induced cirrus anvil clouds.

Acknowledgments. The authors would like to express their appreciation to G. Gibson, A. Cheng, D. Young, and D. Wang for their valuable comments. This re-

search was supported by NASA's Science Mission Directorate through the EOS data analysis and radiation science programs, the CERES mission, and the NASA Energy and Water cycle Studies (NEWS) program. CERES and VIRS products and TMI data were obtained from the NASA Langley Atmospheric Sciences Data Center in Hampton, Virginia, and Goddard Distributed Active Archive Center in Greenbelt, Maryland, respectively.

REFERENCES

- Albritton, D., and Coauthors, 2001: Summary for policymakers. *Climate Change 2001: The Scientific Basis*, J. T. Houghton et al., Eds., Cambridge University Press, 20 pp.
- Braham, R. R., Jr., 1952: The water and energy budgets of the thunderstorm and their relation to thunderstorm development. *J. Meteor.*, **9**, 227–242.
- Breon, F.-M., D. Tanre, and S. Generoso, 2002: Aerosol effect on cloud droplet size monitored from satellite. *Science*, **295**, 834–838.
- Chambers, L., B. Lin, and D. Young, 2002: New CERES data examined for evidence of tropical iris feedback. *J. Climate*, **15**, 3719–3726.
- Chong, M., and D. Hauser, 1989: A tropical squall line observed during the COPT 81 experiment in West Africa. Part II: Water budget. *Mon. Wea. Rev.*, **117**, 728–744.
- Del Genio, A. D., and A. Wolf, 2000: Climatic implications of the observed temperature dependence of the liquid water path of low clouds in the southern Great Plains. *J. Climate*, **13**, 3465–3486.
- , and W. Kovari, 2002: Climatic properties of tropical precipitating convection under varying environmental conditions. *J. Climate*, **15**, 2597–2615.
- , —, M.-S. Yao, and J. Jonas, 2005: Cumulus microphysics and climate sensitivity. *J. Climate*, **18**, 2376–2387.
- Fairall, C., E. F. Bradley, D. P. Rogers, J. B. Edson, and G. S. Young, 1996: Bulk parameterization of air-sea fluxes for TOGA COARE. *J. Geophys. Res.*, **101**, 3747–3764.
- Fankhauser, J. C., 1988: Estimates of thunderstorm precipitation efficiency from field measurements in CCOPE. *Mon. Wea. Rev.*, **116**, 663–684.
- Ferrier, B. S., J. Simpson, and W.-K. Tao, 1996: Factors responsible for different precipitation efficiencies between midlatitude and tropical squall simulations. *Mon. Wea. Rev.*, **124**, 2100–2125.
- Fu, R., A. DelGenio, B. Rossow, and W. T. Liu, 1992: Cirrus-cloud thermostat for tropical sea surface temperatures tested using satellite data. *Nature*, **358**, 394.
- Gamache, J. F., and R. A. Houze Jr., 1983: Water budget of a mesoscale convective system in the tropics. *J. Atmos. Sci.*, **40**, 1835–1850.
- Hartmann, D. L., and M. L. Michelsen, 1993: Large-scale effects on the regulation of tropical sea surface temperature. *J. Climate*, **6**, 2049–2062.
- , and —, 2002: No evidence for iris. *Bull. Amer. Meteor. Soc.*, **83**, 249–254.
- Ho, S.-P., B. Lin, P. Minnis, and T.-F. Fan, 2003: Estimates of cloud vertical structure and water amount over tropical oceans using VIRS and TMI data. *J. Geophys. Res.*, **108**, 4419, doi:10.1029/2002JD003298.
- Houze, R., 1993: *Cloud Dynamics*. Vol. 53, International Geophysics Series, Academic Press, 573 pp.
- Kummerow, C., and Coauthors, 2001: The evolution of the Goddard profiling algorithm (GPROF) for rainfall estimation from passive microwave sensors. *J. Appl. Meteor.*, **40**, 1801–1820.
- Lau, K. M., and H. T. Wu, 2003: Warm rain processes over tropical oceans and climate implications. *Geophys. Res. Lett.*, **30**, 2290, doi:10.1029/2003GL018567.
- Lin, B., and W. B. Rossow, 1996: Seasonal variation of liquid and ice water path in nonprecipitating clouds over oceans. *J. Climate*, **9**, 2890–2902.
- , and —, 1997: Precipitation water path and rainfall rate estimates over oceans using Special Sensor Microwave Imager and International Satellite Cloud Climatology Project data. *J. Geophys. Res.*, **102**, 9359–9374.
- , B. Wielicki, P. Minnis, and W. B. Rossow, 1998a: Estimation of water cloud properties from satellite microwave, infrared, and visible measurements in oceanic environments. I: Microwave brightness temperature simulations. *J. Geophys. Res.*, **103**, 3873–3886.
- , P. Minnis, B. Wielicki, D. R. Doelling, R. Palikonda, D. F. Young, and T. Uttal, 1998b: Estimation of water cloud properties from satellite microwave, infrared, and visible measurements in oceanic environments. II: Results. *J. Geophys. Res.*, **103**, 3887–3905.
- , —, A. Fan, J. A. Curry, and H. Gerber, 2001: Comparison of cloud liquid water paths derived from in situ and microwave radiometer data taken during the SHEBA/FIREACE. *Geophys. Res. Lett.*, **28**, 975–978.
- , B. Wielicki, L. Chambers, Y. Hu, and K.-M. Xu, 2002: The iris hypothesis: A negative or positive cloud feedback? *J. Climate*, **15**, 3–7.
- , P. Minnis, and A. Fan, 2003: Cloud liquid water amount variations with temperature observed during the Surface Heat Budget of the Arctic Ocean (SHEBA) experiment. *J. Geophys. Res.*, **108**, 4427, doi:10.1029/2002JD002851.
- Lindzen, R. S., M.-D. Chou, and A. Hou, 2001: Does the Earth have an adaptive infrared iris? *Bull. Amer. Meteor. Soc.*, **82**, 417–432.
- Lipps, F. B., and R. S. Hemler, 1986: Numerical simulation of deep tropical convection associated with large-scale convergence. *J. Atmos. Sci.*, **43**, 1796–1816.
- Loeb, N., and Coauthors, 2003: Angular distribution models for top-of-atmosphere radiative flux estimation from the Clouds and the Earth's Radiant Energy System instrument on the Tropical Rainfall Measuring Mission satellite. Part I: Methodology. *J. Appl. Meteor.*, **42**, 240–265.
- Lucas, C., E. J. Zipser, and B. S. Ferrier, 2000: Sensitivity of tropical west Pacific oceanic squall lines to temperature, wind, and moisture profiles. *J. Atmos. Sci.*, **57**, 2351–2373.
- Machado, L. A. T., W. B. Rossow, R. L. Guedes, and A. W. Walker, 1998: Life cycle variations of mesoscale convective systems over the Americas. *Mon. Wea. Rev.*, **126**, 1630–1654.
- Mapes, B., 1993: Gregarious tropical convection. *J. Atmos. Sci.*, **50**, 2026–2037.
- Minnis, P., and Coauthors, 1995: Cloud optical property retrieval (subsystem 4.3). Clouds and the Earth's Radiant Energy System (CERES) Algorithm Theoretical Basis Document, Volume III: Cloud Analyses and Radiance Inversions (Sub-

- system 4), CERES Science Team, Eds., NASA Rep. 1376, Vol. 3, 135–176.
- , and Coauthors, 1997: Cloud optical property retrieval (subsystem 4.3). Clouds and the Earth's Radiant Energy System (CERES) Algorithm Theoretical Basis Document, Release 2.2, Update to Minnis et al. (1995). [Available online at <http://asd-www.larc.nasa.gov/ATBD/ATBD.html>.]
- , D. F. Young, B. A. Wielicki, P. W. Heck, X. Dong, L. L. Stowe, and R. Welch, 1999: CERES cloud properties derived from multispectral VIRS data. *Proceedings of the EOS/SPIE Symposium on Remote Sensing*, Vol. 3867, EOS/SPIE, 91–102.
- , —, —, S. Sun-Mack, Q. Z. Trepte, Y. Chen, P. Heck, and X. Dong, 2002: A global cloud database from VIRS and MODIS for CERES. *Proceedings of the SPIE 3rd International Asia-Pacific Environmental Remote Sensing Symposium 2002: Remote Sensing of the Atmosphere, Ocean, Environment, and Space*, Vol. 4891, SPIE, 115–126.
- Oury, S., X. Dou, and J. Testud, 2000: Estimate of precipitation from the dual-beam airborne radars in TOGA COARE. Part II: Precipitation efficiency in the 9 February 1993 MCS. *J. Appl. Meteor.*, **39**, 2371–2384.
- Ramanathan, V., and W. Collins, 1991: Thermodynamic regulation of ocean warming by cirrus clouds deduced from observations of the 1987 El Niño. *Nature*, **351**, 27–32.
- , P. J. Crutzen, J. T. Kiehl, and D. Rosenfeld, 2001: Aerosols, climate and the hydrological cycle. *Science*, **294**, 2119–2124.
- Reynolds, R. W., and T. M. Smith, 1994: Improved global sea surface temperature analysis. *J. Climate*, **7**, 929–948.
- Schulz, J., P. Schluessel, and H. Grassl, 1993: Water vapour in the atmospheric boundary layer over oceans from SSM/I measurements. *Int. J. Remote Sens.*, **14**, 2773–2789.
- , J. Meywerk, S. Ewald, and P. Schluessel, 1997: Evaluation of satellite-derived latent heat fluxes. *J. Climate*, **10**, 2782–2795.
- Shepherd, J. M., B. S. Ferrier, and P. S. Ray, 2001: Rainfall morphology in Florida convergence zones: A numerical study. *Mon. Wea. Rev.*, **129**, 177–197.
- Stephens, G., 2005: Cloud feedbacks in the climate system: A critical review. *J. Climate*, **18**, 237–273.
- Sud, Y. C., and G. K. Walker, 1999: Microphysics of Clouds with the Relaxed Arakawa–Schubert Scheme (McRAS). Part I: Design and evaluation with GATE phase III data. *J. Atmos. Sci.*, **56**, 3196–3220.
- Tao, W.-K., D. Johnson, C.-L. Shie, and J. Simpson, 2004: The atmospheric energy budget and large-scale precipitation efficiency of convective systems during TOGA COARE, GATE, SCSMEX, and ARM: Cloud-resolving model simulations. *J. Atmos. Sci.*, **61**, 2405–2423.
- Tompkins, A. M., 2001: On the relationship between tropical convection and sea surface temperature. *J. Climate*, **14**, 633–637.
- Tselioudis, G., D. Rind, and W. Rossow, 1992: Global patterns of cloud optical thickness variation with temperature. *J. Climate*, **5**, 1642–1657.
- Wallace, J., 1992: Effect of deep convection on the regulation of tropical sea surface temperature. *Nature*, **357**, 230–231.
- Weisman, M. L., and J. B. Klemp, 1982: The dependence of numerically simulated convective storms on vertical wind shear and buoyancy. *Mon. Wea. Rev.*, **110**, 504–520.